



Magnetochemical effects on phase stability and vacancy formation in fcc Fe-Ni alloysKangming Li , Chu-Chun Fu , Maylise Nastar, and Frédéric Soisson *Université Paris-Saclay, CEA, Service de Recherches de Métallurgie Physique, F-91191 Gif-sur-Yvette, France*Mikhail Yu. Lavrentiev *United Kingdom Atomic Energy Authority, Culham Science Centre, Abingdon, Oxon OX14 3DB, United Kingdom*

(Received 13 January 2022; accepted 24 June 2022; published 8 July 2022)

We investigate phase stability and vacancy formation in fcc Fe-Ni alloys over a broad composition-temperature range, via a density functional theory parametrized effective interaction model, which includes explicitly spin and chemical variables. On-lattice Monte Carlo simulations based on this model are used to predict the temperature evolution of the magnetochemical phase. The experimental composition-dependent Curie and chemical order-disorder transition temperatures are successfully predicted. We point out a significant effect of chemical and magnetic orders on the magnetic and chemical transitions, respectively. The resulting phase diagram shows a magnetically driven phase separation around 10–40% Ni and 570–700 K, between ferromagnetic and paramagnetic solid solutions, in agreement with experimental observations. We compute vacancy formation magnetic free energy as a function of temperature and alloy composition. We identify opposite magnetic and chemical disordering effects on vacancy formation in the alloys with 50% and 75% Ni. We find that thermal magnetic effects on vacancy formation are much larger in concentrated Fe-Ni alloys than in fcc Fe and Ni due to a stronger magnetic interaction.

DOI: [10.1103/PhysRevB.106.024106](https://doi.org/10.1103/PhysRevB.106.024106)**I. INTRODUCTION**

Magnetism is an indispensable ingredient for understanding and predicting properties in Fe and Fe-based alloys. It plays a crucial role in phase stability and the bcc-fcc phase transition in Fe [1–5]. In Fe-based alloys, the magnetochemical interplay can lead to a change of the chemical order-disorder transition temperature, local segregation, or unmixing tendency [6–9]. Thermal magnetic effects are also known to have an impact on vacancy properties and atomic diffusion in bcc Fe [10–13].

Effects of magnetism can be obtained via first-principles calculations, which are routinely performed in magnetically ordered systems. However, it remains a challenging task to model magnetic excitations and paramagnetism [14]. First-principles approaches to simulate finite-temperature magnetism in alloys include, for instance, the disordered local moment (DLM) and partial DLM methods [15–18] and the spin-wave method [19]. However, these approaches generally require additional interpolation schemes such as the semiempirical Ruch model [20] to obtain the temperature evolution of magnetic and energetic properties. Furthermore, they are too computationally expensive for a systematic exploration of the spin-atom configurational space of magnetic alloys. On the other hand, while upper-scale atomistic approaches such as spin-lattice dynamics [21,22] and spin-atom Monte Carlo simulations [23–25] provide an efficient way to investigate finite-temperature magnetic effects, it is generally difficult to develop accurate models and potentials for concentrated alloys with the presence of structural defects.

This work is focused on fcc Fe-Ni alloys, which are the basis of austenitic steels. The alloy with around 50% and 75% Ni has a ferromagnetic $L1_0$ and $L1_2$ ordered structure, respectively, at low temperatures. They undergo successive chemical and magnetic transitions with increasing temperature [26,27]. A strong magnetochemical interplay is expected and can have an impact on the phase stability and properties of structural defects.

The phase stability of this system has been extensively investigated experimentally and theoretically [24,26–35]. However, thermodynamic measurements of, e.g., activity coefficients and formation enthalpies were performed only in paramagnetic and chemically disordered alloys [26,29]. It is difficult to estimate the magnetic contribution to phase stability based directly on experimental information. On the theoretical side, magnetic effects on the phase stability of fcc Fe-Ni alloys were studied using model Hamiltonians combined with on-lattice Monte Carlo simulations, showing a significant impact on the chemical order-disorder transition temperatures [33–35]. However, the Ising or Heisenberg models adopted in these studies [33–35] were developed only for specific compositions, and the composition dependence of magnetic moments as well as the thermal longitudinal spin fluctuations were not taken into account. Recently, a magnetic cluster expansion model was parametrized for the whole composition range of fcc Fe-Ni alloys [24], but the predicted Curie points of the disordered alloys are found to be much lower than the experimental data.

As the simplest structural defect in metals and alloys, vacancy plays a dominant role in atomic diffusion. Knowledge

of vacancy formation properties is thus crucial for the understanding of kinetic processes. From a general point of view, theoretical studies addressing finite-temperature magnetic effects on vacancy formation properties have been focused on metals and extremely dilute Fe alloys [11–13,18,36–39]. By contrast, vacancy formation energies in concentrated alloys are often computed with the magnetic ground states [40–46] or, less commonly, in the ideal paramagnetic state [16]. In addition, the investigations of the alloying effects on vacancy formation energies are restricted to either nearly perfect ordered phases [47–52] or fully random solid solutions [40–46,53–55]. A continuous and comprehensive modeling of vacancy properties as a function of temperature and hence of chemical and magnetic orders is still missing. It is noted that Girifalco [56] and Ruch *et al.* [20] proposed to express vacancy formation free energy G_f as a function of order parameter S :

$$G_f(S) = (1 + \alpha S^2) \cdot G_f(0), \quad (1)$$

where α is a system-dependent parameter, S is the chemical or magnetic long-range order parameter, and $G_f(0)$ is the vacancy formation free energy in the chemically or magnetically disordered state. However, these interpolation schemes are not applicable to the alloy systems with simultaneous chemical and magnetic evolutions.

There are few theoretical and experimental studies on vacancy properties in fcc Fe-Ni alloys. Zhao *et al.* [46] used density functional theory (DFT) calculations to obtain the distribution of vacancy formation energies in the ferromagnetic disordered structures with 50% and 80% Ni, and compared the DFT results with the predictions from empirical potentials. Caplain and Chambron measured vacancy formation energies in Fe-Ni disordered alloys with 50–94% Ni using the magnetic anisotropy method [57,58]. However, the effects of magnetic and chemical orders on vacancy properties remain largely unexplored experimentally and theoretically. Besides, a comprehensive atomic-scale modeling of the vacancy properties as a function of temperature and hence of chemical and magnetic orders is still missing.

This study is aimed at elucidating the magnetochemical effects on phase stability and vacancy formation in fcc Fe-Ni alloys. We develop an effective interaction model, which is parametrized on DFT results only and includes explicit chemical and magnetic variables. We treat the magnetic interaction within a generalized Heisenberg formalism [24,59] to account for the dependence of magnetic moments on local chemical composition and the strong longitudinal spin fluctuations in this system [32,39,60]. The model combined with on-lattice Monte Carlo simulations enables one to fully take into account the simultaneous magnetic and chemical evolutions with temperature on the whole composition range of the Fe-Ni alloys.

The paper is organized as follows. Details of the DFT calculations, model parametrization, and Monte Carlo simulations are given in Sec. II. Phase stability predictions, including chemical and magnetic transition temperatures, phase diagram, and magnetochemical interplay, are presented in Sec. III. The temperature and concentration dependences of vacancy formation magnetic free energy are discussed in Sec. IV.

II. COMPUTATIONAL DETAILS

As a first step, we performed DFT calculations, presented in Sec. II A. Then, these results were used for the parametrization of the effective interaction model, as detailed in Sec. II B. Finally, several Monte Carlo schemes, as described in Sec. II C, were employed to study the phase stability and vacancy formation properties in fcc Fe-Ni alloys.

A. DFT calculations

DFT calculations were performed using the projector augmented wave (PAW) method [61,62] as implemented in the Vienna Ab-initio Simulation Package (VASP) code [63–65]. The generalized gradient approximation (GGA) for the exchange-correlation functional in the Perdew-Burke-Ernzerhof (PBE) parametrization [66] was employed. $3d$ and $4s$ electrons of Fe and Ni atoms were considered as valence electrons. The plane-wave basis cutoff was set to 400 eV. The Methfessel-Paxton broadening scheme with a smearing width of 0.1 eV was used [67]. The convergence cutoff for the electronic self-consistency loop was set to 10^{-6} eV. The k -point grids were adjusted according to the cell size to achieve a sampling density equivalent to a cubic unit cell with a 16^3 shifted grid following the Monkhorst-Pack scheme [68]. Atomic magnetic moments were obtained by an integration of spin-up and spin-down charge densities within the PAW spheres, with a radius of 1.302 Å for Fe and 1.286 Å for Ni.

Random solid solutions were represented by special quasirandom structures (SQSs) [69] with minimized atomic short-range order parameters [70,71]. Supercells of various sizes (up to 128 atoms) were used for vacancy-free systems. For vacancy-containing alloys, 108-site and 128-site supercells were used.

In our previous work [32], DFT calculations had been performed in the Fe-Ni alloys with the respective magnetic ground states, in which the atomic positions, cell shapes, and volumes were optimized. In this study, we explored via DFT various magnetic states of the fcc Fe-Ni structures, namely, magnetically ordered structures, magnetically partially ordered structures, and magnetic SQSs. Furthermore, the local magnetic moment constraint [8] is also applied, for instance, to ferromagnetic and antiferromagnetic structures and magnetic SQSs of Fe and Ni (0.1 – $0.9 \mu_B$ for Ni and 0.1 – $3.5 \mu_B$ for Fe). For these configurations, the atomic positions were fixed to those in the magnetic ground states, while the cell shape and volume were optimized.

B. Effective interaction model

In our previous work, effective interaction models (EIMs) were parametrized for pure fcc Fe and Ni systems, respectively [39]. In this work, they are unified and extended as a single EIM for the whole composition range of fcc Fe-Ni alloys. The Hamiltonian form is similar to the previous ones used to investigate magnetic properties, phase stability [24,72,73], and vacancy formation and diffusion properties [13,59] of the Fe-based systems. The current EIM has the

following form:

$$H = \sum_i \sigma_i \cdot \underbrace{\left(A_i M_i^2 + B_i M_i^4 + \sum_j \sigma_j \cdot J_{ij} \mathbf{M}_i \mathbf{M}_j \right)}_{\text{magnetic}} + \sum_i \sigma_i \cdot \underbrace{\left[\epsilon_i + \sum_j \sigma_j \cdot (V_{ij} + \alpha_{ij} T) \right]}_{\text{chemical (nonmagnetic)}}, \quad (2)$$

where i denotes the i th fcc lattice site, σ_i is the occupation variable and is equal to 1 (or 0) for an occupied (or vacant) lattice site, and \sum_j is a sum over all the neighboring sites up to the fourth-neighbor shell.

In the magnetic part of the Hamiltonian, M_i is the local magnetic moment, A_i and B_i are the on-site magnetic parameters, and J_{ij} are the exchange interaction parameters.

In the nonmagnetic part, ϵ_i is the on-site nonmagnetic parameter, V_{ij} and α_{ij} are the nonmagnetic interaction parameters, and T is the absolute temperature. Indeed, the impact of vibrational entropies of mixing on the phase stability of fcc Fe-Ni structures is shown to be significant [32,74]. In the present rigid-lattice EIM, we choose a rather simple way to incorporate these effects: we introduce the nonmagnetic parameters α_{ij} to account for the vibrational entropies of mixing of the ferromagnetic structures, which were computed in our previous work within the harmonic approximation [32]. This simple treatment neglects the possible magnon-phonon coupling [75] and amounts to integrating the contribution from the fast vibrational degrees of freedom into the nonmagnetic pair interactions. The nonmagnetic interactions thus become the pair free energies [76–79], instead of the simple pair energies of the usual models, due to the inclusion of the entropic contribution. We are aware that the characteristic timescales of the magnon and phonon excitations may not be very different [14,80]. On the other hand, our EIM is not parametrized to capture the vibrational contribution to vacancy formation. Instead, vacancy formation vibrational entropy is computed *a posteriori* from DFT calculations. A more sophisticated treatment for the vibrational degree of freedom in concentrated alloys is beyond the scope of the present study.

The DFT database for fitting the present EIM includes around 1200 different structures, covering various (both chemically and magnetically) ordered, partially ordered, and disordered structures (SQSS). For the magnetic and chemical interaction parameters, we introduce a linear dependence on the local concentration and a dependence on the distance from the vacancy, in order to capture the concentration-dependent interactions and the effects of the vacancy (see the Supplemental Material [81]). The resulting EIM has 43 parameters for the vacancy-free systems and, additionally, 26 parameters for the vacancy-containing systems. The standard deviation of the fitted energies per atom is around 14 meV/atom and the standard deviation of the fitted vacancy formation energies is around 35 meV/atom. Details of the model parametrization can be found in the Supplemental Material [81].

C. Monte Carlo simulations

Temperature-dependent properties are determined from the EIM combined with on-lattice Monte Carlo (MC) simulations,

using 16^3 fcc unit cells containing 16 384 lattice sites. Some of these properties are defined as follows.

All the alloy concentrations are expressed in the Ni atomic fraction. Following the Warren-Cowley formulation [70], the atomic short-range order (ASRO) parameter for the n th coordination shell is calculated as follows:

$$\text{ASRO}_n = 1 - \frac{x_{\text{Ni}}^n}{x_{\text{Ni}}}, \quad (3)$$

where x_{Ni} is the nominal Ni concentration and x_{Ni}^n is the average local Ni concentration in the n th coordination shell of Fe atoms. The atomic long-range order (ALRO) parameter for L1₀-FeNi and L1₂-FeNi₃ is defined as

$$\text{ALRO} = \frac{N_{\text{Fe}}^{\text{Fe}}}{N_{\text{Fe}}} - \frac{N_{\text{Fe}}^{\text{Ni}}}{N_{\text{Ni}}}, \quad (4)$$

where N_{Fe} and N_{Ni} are the total numbers of Fe and Ni, respectively, and $N_{\text{Fe}}^{\text{Fe}}$ and $N_{\text{Fe}}^{\text{Ni}}$ are the numbers of Fe in the Fe and Ni sublattices, respectively. The Curie temperature T_{Curie} is estimated as the inflection point of the following function [72] fitted to the obtained magnetization values:

$$\frac{M(T)}{M(T=1K)} = (1 - aT) \frac{1 + \exp\left(-\frac{b}{c}\right)}{1 + \exp\left(\frac{T-b}{c}\right)}. \quad (5)$$

For vacancy-free systems, we use three types of MC schemes for different purposes: spin Monte Carlo (SMC), spin-atom canonical Monte Carlo (CMC), and semi-grand-canonical Monte Carlo (SGCMC) [79]. In SMC simulations, the atomic configuration is fixed while the magnetic configuration evolves with temperature. SMC simulations are used to obtain magnetic properties (e.g., magnetization, magnetic short-range order, and T_{Curie}) for a fixed atomic configuration. In CMC simulations, the chemical composition is fixed, while the atomic and magnetic configurations are equilibrated. CMC simulations allow one to determine magnetic properties, the ALRO and ASRO parameters of the equilibrium phase for a given Ni concentration and temperature. SGCMC simulations are used as a convenient way to construct the phase diagram and its principle can be found in Refs. [78,79,82].

In principle, quantum statistics should be used for the magnetic degree of freedom below the magnetic transition temperature. This has been previously done for the pure systems [12,13,39,83], but a systematic application to alloys can be quite complicated and involve further approximations. In this study, classical statistics is used to control the magnetic and chemical evolutions in alloys for the whole composition range.

For vacancy-containing systems, we compute the vacancy formation free energy G_f , which is linked to the equilibrium vacancy concentration $[V]_{\text{eq}}$ via

$$[V]_{\text{eq}} = \exp\left(-\frac{G_f}{k_{\text{B}}T}\right), \quad (6)$$

where G_f can include all the nonconfigurational entropic contributions. To evaluate G_f , we use a Widom-type MC scheme [84–86], in which the free-energy difference $G_1 - G_0$ between the system 1 and 0 is computed as

$$G_1 - G_0 = -k_{\text{B}}T \ln \left\langle \exp\left(-\frac{E_1 - E_0}{k_{\text{B}}T}\right) \right\rangle_0, \quad (7)$$

where E_1 and E_0 are the energies of the two systems in the same microstate, and $\langle \cdot \rangle_0$ denotes the ensemble average of $\exp(-\frac{E_1 - E_0}{k_B T})$ in the system 0. If there is the same number of atoms in the system 1 as in the system 0, and if there is one vacancy in the system 1 and no vacancy in the system 0, the free-energy difference from Eq. (7) is equal to G_f . The details of the scheme are given in the Supplemental Material [81].

Please note that our EIM is not parametrized to predict the vacancy formation vibrational entropy S_f^{vib} . Therefore, what is directly predicted from our EIM is the vacancy formation magnetic free energy G_f^{mag} , which includes finite-temperature effects due to magnetic and chemical excitations. On the other hand, we adopt a very simplified treatment for S_f^{vib} : we compute it in the magnetic ground states of fcc Fe and Ni from DFT, and use a linear interpolation with respect to concentration to obtain S_f^{vib} in concentrated alloys, which is then added *a posteriori* to the EIM results to obtain the complete $G_f (= G_f^{\text{mag}} - T S_f^{\text{vib}})$. Indeed, accurately computing S_f^{vib} in concentrated alloys involves various challenging issues in DFT and MC and necessitates a dedicated study. Therefore, this paper is focused on finite-temperature magnetochemical effects on vacancy formation free energy.

III. PHASE STABILITY OF FCC FE-NI ALLOYS

This section is focused on the phase stability prediction from the EIM for vacancy-free fcc Fe-Ni alloys. First, we validate our EIM by comparing its predictions to experimental data. We also compare the vibrational and magnetic entropic contributions to the chemical transitions. Then, we discuss the calculated fcc phase diagram with other theoretical results. In the last section, we elucidate the interplay between magnetic and chemical degrees of freedom.

A. Magnetic and chemical transition temperatures

In the following, we evaluate the accuracy of the EIM by a comparison of the predicted magnetic and chemical transition temperatures with the experimental values. A comparison of ground-state magnetic, energetic properties, and vibrational entropies of mixing between the EIM and DFT results is also given in the Supplemental Material [81].

According to the EIM, the fcc random solid solutions with more than 20% Ni have a collinear ferromagnetic (FM) ground state (see the Supplemental Material [81]). Figure 1 shows the predicted and experimental T_{Curie} . The experimental T_{Curie} were measured in the samples quenched from 923 to 1273 K [87,88] with nonzero ASRO. Our SMC results of T_{Curie} are obtained with the fully random structures (ASRO equal to zero), whereas the CMC results are obtained with the equilibrium spin-atom structures which have stronger ASRO than the experimental samples. The predicted Curie temperatures of the experimental samples should therefore lie between the CMC and SMC curves.

In alloys with $x_{\text{Ni}} > 0.45$, the CMC results of T_{Curie} are in very good agreement with the experimental data in Fig. 1, while the SMC results are slightly lower. This indicates that the experimental ASRO is closer to that of the equilibrium structures obtained in CMC simulations than the zero ASRO of the random alloys. However, the CMC results show a large

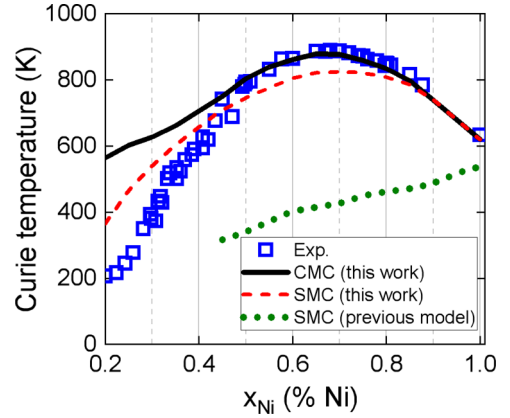


FIG. 1. T_{Curie} of fcc random solid solutions from the experiments [87–89], the current EIM, and the previous model in Ref. [24]. The spin Monte Carlo results in Ref. [24] are reported only for 50% and 75% Ni; here we compute the values for other concentrations using their model.

deviation from the experimental data in alloys with $x_{\text{Ni}} < 0.4$. Indeed, the predicted equilibrium structures around 10–40% Ni at 570–700 K consist of two different disordered phases, as will be shown in Sec. III B. Therefore, the structures from the CMC simulations do not correspond to the experimental homogeneous disordered samples. Meanwhile, the difference between the SMC results and experimental T_{Curie} in alloys with $x_{\text{Ni}} < 0.3$ may be due to the nonzero ASRO in the measured samples. In addition, as the Invar region is not even perfectly clear from first-principles studies (e.g., concerning the magnetic ground states [32,90]), we prioritize the model description for the Ni-rich alloys, and hence our model may describe less well the properties in the alloys very rich in Fe.

The ordered structures $L1_0$ -FeNi and $L1_2$ -FeNi₃ have a FM ground state, with the experimental T_{Curie} higher than those in the disordered alloys of the same compositions. This point is well reproduced by the EIM predictions, which compare favorably with the experimental results, as shown in Table I.

The chemical order-disorder transition temperatures T_{chem} at 50% and 75% Ni are obtained from the CMC simulations. As shown in Fig. 2, the ALRO parameter changes abruptly around 598 K and 766 K at 50% and 75% Ni, respectively, in excellent agreement with the experimental T_{chem} of 593 K at 50% Ni [94] and of 770–790 K at 75% Ni [93,95,96]. Above T_{chem} , the equilibrium structures are found to still retain a degree of ASRO.

We find that T_{chem} at 50% and 75% Ni are increased by 332 K and 154 K, respectively, if the vibrational contribution is switched off in the EIM. This confirms the strong vibrational effects on the chemical transitions in fcc Fe-Ni

TABLE I. Comparison of T_{Curie} of $L1_0$ -FeNi and $L1_2$ -FeNi₃ between the EIM prediction from SMC simulations and the experiments.

	This work	Expt.
$L1_0$ -FeNi	845 K	840 K [91]
$L1_2$ -FeNi ₃	968 K	954 K [92], 940 K [93]

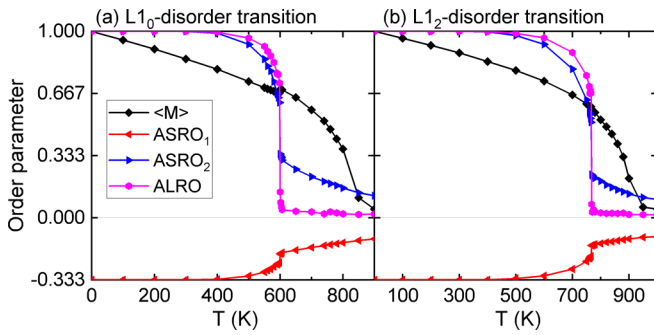


FIG. 2. Predicted temperature evolution of the reduced magnetization, the ASRO (of the first two shells) and ALRO parameters in the alloys with (a) 50% and (b) 75% Ni.

alloys as suggested in our previous DFT study [32]. As shown in Table II, the previous DFT study showed that considering only the ideal configurational entropy leads to a largely overestimated values of T_{chem} , whereas a reasonable estimation of T_{chem} can be obtained if vibrational entropies of mixing are included. The effects of magnetic excitations, which are neglected in the previous DFT study [32] but are accounted for in the EIM, are found to have a smaller impact than the vibrational contribution.

One of the motivations of developing the present EIM is to improve the phase stability prediction of the previous fcc Fe-Ni model in Ref. [24]. For instance, the predicted T_{Curie} from this previous model in the disordered structures show a linear dependence on alloy composition and are lower than the experimental data, as shown in Fig. 1. In addition, T_{chem} in the structures with 50% and 75% Ni concluded in Ref. [24] are higher than the corresponding T_{Curie} , in contradiction with the experimental results. These inconsistencies are fixed in the present EIM, which gives a correct prediction of both the magnetic and chemical transition temperatures.

B. Fcc Fe-Ni phase diagram

The phase diagram is constructed by means of the SGCMC simulations. Figure 3 shows the fcc Fe-Ni phase diagram predicted by the EIM, compared with those from the DFT [32] and CALPHAD [27] studies. Though, experimentally, the bcc Fe-Ni phase plays an increasingly important role below 10% Ni [27,29], its consideration is beyond the scope of the present fcc lattice-based study. In the following, we denote $L1_0$ and $L1_2$ as the ordered phases around 50% and 75% Ni, respectively, and γ_{FM}

TABLE II. Chemical order-disorder transition temperatures (in K) in the alloys with 50% and 75% Ni. The contributions considered in the calculations are indicated in the parentheses.

	50% Ni	75% Ni
DFT [32] (conf)	920	1030
DFT [32] (conf+vib)	640	830
EIM, this work (conf+mag)	930	920
EIM, this work (conf+vib+mag)	598	766
Expt. [93–96]	593	770–790

and γ_{PM} as the FM and paramagnetic (PM) solid solutions, respectively.

According to the EIM prediction, the phase diagram below 570 K consists of four monophasic regions (Fe-rich γ_{PM} , $L1_0$, $L1_2$, and Ni-rich γ_{FM}), which are separated by three corresponding biphasic regions. From 570 to 600 K, the biphasic region $\gamma_{\text{PM}} + L1_0$ is replaced by the biphasic regions $\gamma_{\text{FM}} + L1_0$ and $\gamma_{\text{PM}} + \gamma_{\text{FM}}$, which disappear at 600 K and 700 K, respectively. The $L1_0$ - and $L1_2$ -disorder transitions at 50% and 75% Ni occur at 600 and 776 K, respectively.

The major difference between the EIM-predicted phase diagram and the DFT one [32] is the absence of γ_{PM} in the latter, which considered fully FM phases only. On the other hand, there is no significant difference in the other parts of the two phase diagrams involving the ordered phases. This is not surprising considering the high Curie temperatures of the ordered phases, which remain FM up to the order-disorder transition temperatures.

Recently, Ohnuma *et al.* [27] determined experimentally the phase equilibria in Fe-Ni alloys between 673 K and 973 K and revised the thermodynamic descriptions in the CALPHAD modeling. In particular, the $L1_0$ -disorder transition temperature is predicted to be 550 K using the revised CALPHAD parameters, in better agreement with the experimental value of 593 K [94,97] than the previous CALPHAD prediction of 313 K by Cacciamani *et al.* [29]. The fcc phase diagram calculated with the revised CALPHAD parameters of Ohnuma *et al.* [27] is presented in Fig. 3. Despite some differences in the phase boundaries involving the paramagnetic phase, the calculated phase diagrams from EIM and CALPHAD are similar overall. Both predict a small two-phase region between γ_{FM} and $L1_0$, and a triangle-shape miscibility gap between the ferromagnetic and paramagnetic random alloys. The miscibility gap is consistent with the observations of chemical and magnetic clusters in the Invar alloys [98–101], in which the Ni-rich and Fe-rich local regions are suggested to be ferromagnetic and paramagnetic, respectively [99,100]. This miscibility gap will be discussed in more detail in the next section.

C. Interplay between chemical and magnetic orders

Magnetization is known to have an impact on the chemical order-disorder transition temperature [6,34]. To study how different magnetic states influence the chemical transitions, we control the magnetic state with a temperature T_{spin} different from the temperature controlling the chemical evolution. To do so, we adopt the adiabatic approximation for the magnetic degree of freedom, namely, assuming that the magnon excitations are faster than the chemical evolution. Here we consider two extreme cases for the magnetic state, namely, the magnetic ground state and the PM state.

Table III shows the chemical transition temperatures in the alloys with 50% and 75% Ni with different magnetic states. In the alloy with 75% Ni, the predicted transition temperature ranges from 715 K to 885 K depending on the magnetic state of the system. A strong ferromagnetic order as in the magnetic ground state tends to further stabilize the ordered alloy over the disordered one, while the paramagnetic order reduces the phase stability of $L1_2$ -FeNi₃. On the other hand, the trend is

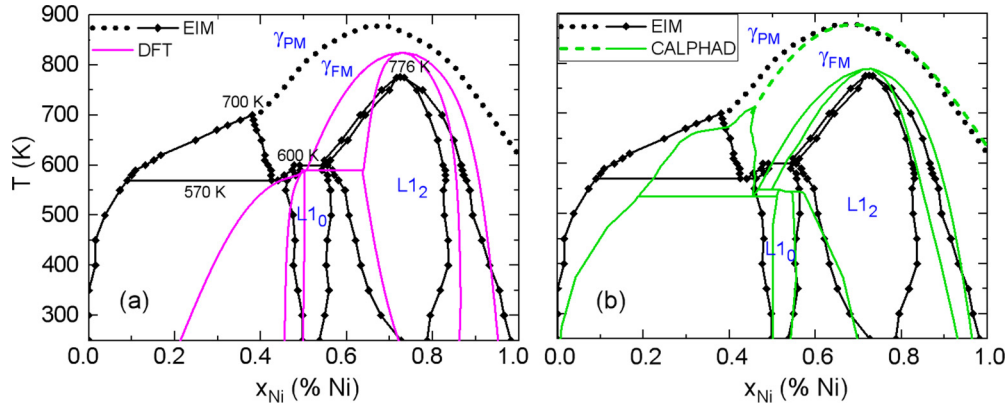


FIG. 3. The fcc Fe-Ni phase diagram predicted by the present EIM, compared to the fcc phase diagrams from (a) our previous DFT study [32] and (b) the CALPHAD study by Ohnuma *et al.* [27]. Here the CALPHAD phase diagram is computed for the present study by using the parameters of the fcc phases given in Ref. [27], in which only the stable bcc-fcc phase diagram was reported.

reversed in the alloy with 50% Ni. In addition, the influence of the magnetic state on the $L1_0$ -disorder transition temperature is less important than on the $L1_2$ -disorder transition temperature.

We have shown that there is a phase separation in the phase diagram around 10–40% Ni and 570–700 K. To observe the phase separation in a canonical system, the equilibrium structure for a given composition is obtained from CMC simulations. The compositions of the coexisting phases are then estimated from the distribution of local Ni concentration [72], which is computed for each fcc lattice site as the atomic fraction of Ni atoms within the fifth coordination shell.

Figure 4(a) shows such distributions in the equilibrium spin-atom structures at 600 K. According to our computed phase diagram, the two-phase composition range at 600 K is between 14% and 40% Ni, as indicated by the vertical lines in Fig. 4(a). For the equilibrium structures with 14% and 40% Ni, we observe a single peak centered on the nominal composition, which is the signature of a homogeneous single-phase system. At intermediate concentration, the distribution exhibits two peaks, indicating the compositions of the two separated phases, namely, 14% and 40% Ni.

The phase separation may be chemically driven, with the magnetic state simply following the composition of the separated phase, or it may be magnetically driven. To elucidate this point, we study the phase equilibrium in the coexistence region by constraining the magnetic state of the system. Four types of constraints are considered, namely, the FM state, the nonmagnetic (NM) state, the magnetic ground state (GS), and the fully paramagnetic (PM) state. Figure 4(b)

TABLE III. Chemical order-disorder transition temperatures (in K) in the alloys with 75% and 50% Ni, obtained with different magnetic states. EQ: equilibrium magnetic state. GS: magnetic ground state within the adiabatic approximation ($T_{\text{spin}} = 1$ K). PM: paramagnetic state within the adiabatic approximation ($T_{\text{spin}} = 1500$ K).

Composition	EQ	GS	PM
75% Ni	766	885	715
50% Ni	598	555	610

presents the resulting distributions of local Ni concentration in the equilibrium structures with nominal 35% Ni at 600 K. The distributions obtained in the FM, GS, and PM states exhibit one single peak at the nominal concentration, while those obtained in the equilibrium magnetic state and the NM state exhibit two peaks but at different locations. Thereby, there are three different equilibrium atomic states. The equilibrium atomic structure in the NM state is practically a phase separation between fcc Fe and Ni, in line with the positive mixing energies of the nonmagnetic fcc solid solutions. From these results, we conclude that the phase separation between γ_{PM} and γ_{FM} is driven by the magnetic interactions.

On the other hand, the magnetic properties of the alloy with a given composition depend on both the atomic long-range and short-range orders (ALRO and ASRO, respectively). In order to perform a quantitative analysis of such effects, we extract from the CMC simulations 10 different chemical configurations of the 75% Ni alloy. These structures are representative of the perfect $L1_2$ ordered structure and the fully random alloy, as well as other intermediate states. For these atomic configurations, we run SMC simulations to equilibrate the magnetic state and measure the corresponding Curie temperature.

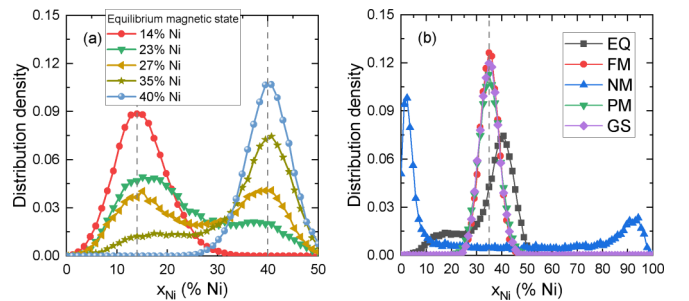


FIG. 4. Distribution of local Ni concentration at 600 K. (a) Equilibrium structures with various Ni content, without constraining the magnetic state. (b) Equilibrium structures with 35% Ni. EQ: equilibrium magnetic state. FM: ferromagnetic. NM: nonmagnetic. PM: paramagnetic within adiabatic approximation ($T_{\text{spin}} = 1500$ K). GS: magnetic ground state within adiabatic approximation ($T_{\text{spin}} = 1$ K).

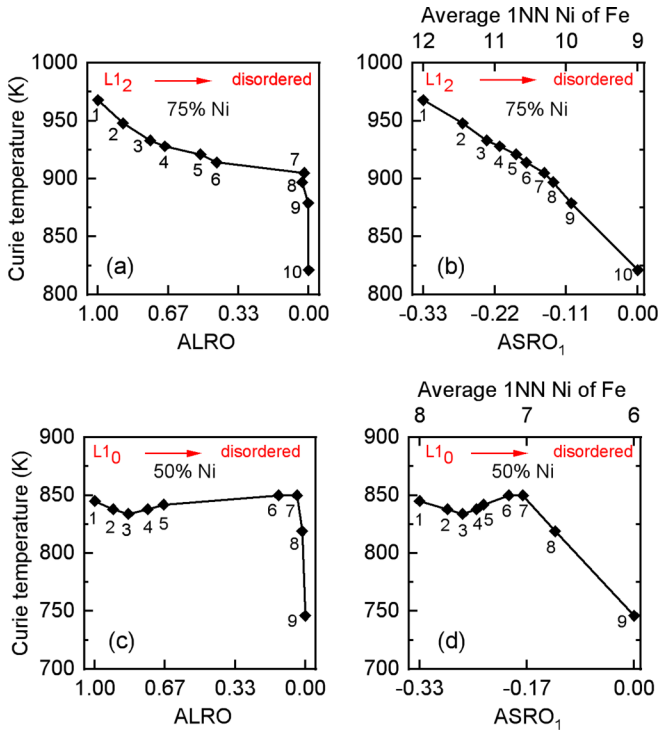


FIG. 5. Curie temperatures as functions of ALRO and ASRO₁ in the structures with (a), (b) 75% Ni and (c), (d) 50% Ni. The numbers beside the symbols are used to label the same chemical configuration. The top X axis in (b) and (d) indicates the corresponding average number of first nearest Ni neighbors for an Fe atom.

Figure 5 shows the Curie temperatures of these structures as functions of ALRO and the atomic short-range order of the first shell (ASRO₁). The ordering of the configurations is the same in the two figures [e.g., the fifth data from the left in (a) and (b), or in (c) and (d), correspond to the same structure]. The Curie temperature decreases from 968 K in the perfect L₁₂ structure to 821 K in the completely disordered one. For structures with vanishing ALRO, their Curie temperatures can still differ by as much as about 80 K due to the remaining ASRO. Indeed, it is found that the Curie temperatures have a rather linear dependence on ASRO₁ [Fig. 5(b)]. A similar investigation is also performed at 50% Ni [Figs. 5(c) and 5(d)]. The Curie temperatures are found to be similar among the ordered structures (ALRO > 0), whereas they are more sensitive to the variation in the ASRO₁ in the disordered state (ALRO = 0).

IV. VACANCY FORMATION PROPERTIES IN fcc Fe-Ni ALLOYS

A. Accuracy of the model for vacancy-containing systems

The present EIM is based on our previously developed EIMs of fcc Fe and Ni (namely, the previous model parameters are kept), whose accuracy has been demonstrated in a previous study [39]. In the following, we validate the EIM description of vacancy-containing Fe-Ni alloys by comparing its predicted vacancy formation energies with DFT results in the ordered and disordered structures.

TABLE IV. Vacancy and antisite formation energies (in eV) in the Fe and Ni sublattices calculated from DFT and EIM for the stoichiometric L₁₂-FeNi₃ and L₁₀-FeNi structures at the 0 K limit. V_{Fe} and Ni_{Fe} denote a vacancy and a Ni antisite in the Fe sublattice, respectively.

	L ₁₂ -FeNi ₃		L ₁₀ -FeNi	
	DFT	EIM	DFT	EIM
V _{Fe}	1.392	1.300	1.897	1.561
V _{Ni}	1.593	1.666	1.847	1.794
Fe _{Ni}	0.256	0.287	0.275	0.253
Ni _{Fe}				

Calculating vacancy formation energies in alloys from DFT is nontrivial because chemical potentials in alloys cannot be obtained in a straightforward way as in pure systems. In an ordered phase with a dilute amount of point defects (e.g., vacancies and antisites), chemical potentials and point-defect formation energies can be calculated within the grand canonical ensemble formalism [47,50] or the canonical ensemble formalism [48,49,51,52]. Here we use the canonical ensemble formalism, which was first proposed by Hagen and Finnis [48] and further developed by Mishin and Herzig [49], to compute vacancy and antisite formation energies. The results calculated using the DFT and EIM data are shown in Table IV.

First, it can be seen that the antisite formation energies are much lower than the vacancy formation energies in the Fe-Ni ordered structures. The Fe-Ni ordered structures are therefore the so-called antisite-disorder compounds, which have been studied in detail by Mishin and Herzig [49]. In particular, it is shown that the antisite formation energies in the two sublattices are equal in antisite-disorder compounds [49].

As shown in Table IV, there is a reasonable agreement between the DFT and EIM predictions of the vacancy formation energies in the Fe and Ni sublattices of L₁₂-FeNi₃ and in the Ni sublattice of L₁₀-FeNi, while the EIM result in the Fe sublattice of L₁₀-FeNi is underestimated by 0.34 eV compared with the DFT one.

In concentrated disordered alloys, it is customary to calculate the local vacancy formation energy at site *i* as [41,43,46,55] E_f^i ,

$$E_f^i = E_{\text{tot},V_i} - E_{\text{tot},0} + \mu, \quad (8)$$

where $E_{\text{tot},0}$ is the energy of the system without a vacancy, E_{tot,V_i} is the energy of the system with a vacancy at site *i*, and μ is the chemical potential of the removed atom in the system. In the DFT-SQS approach, μ is often calculated via the Widom substitution [43,46,84], which requires a large number of atom substitutions at different sites. Since our objective is to validate the present EIM, we may consider the arithmetic average of vacancy formation energy $\langle E_f^i \rangle$, which can be readily obtained from the DFT data without calculating μ . Indeed, the relation $E_{\text{tot},0} = N(x_A\mu_A + x_B\mu_B)$ allows one to

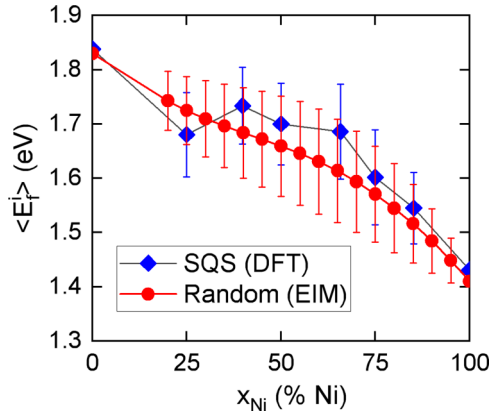


FIG. 6. Average vacancy formation energy as a function of Ni concentration for the random Fe-Ni structures in the magnetic ground state. The error bars denote the standard deviations of local vacancy formation energies.

eliminate μ_A and μ_B in $\langle E_f^i \rangle$ [41]:

$$\begin{aligned} \langle E_f^i \rangle &= x_A (\langle E_{\text{tot}, V_A} \rangle - E_{\text{tot}, 0} + \mu_A) \\ &\quad + x_B (\langle E_{\text{tot}, V_B} \rangle - E_{\text{tot}, 0} + \mu_B) \\ &= x_A \langle E_{\text{tot}, V_A} \rangle + x_B \langle E_{\text{tot}, V_B} \rangle - \frac{N-1}{N} E_{\text{tot}, 0}, \end{aligned} \quad (9)$$

where $\langle E_{\text{tot}, V_A} \rangle$ is the average energy of the system with an A atom removed.

A comparison of $\langle E_f^i \rangle$ in the random Fe-Ni structures between the DFT and EIM predictions is given in Fig. 6. The DFT results are obtained with the 108-site SQSs. For each SQS, nine different Fe and Ni sites are considered to obtain $\langle E_{\text{tot}, V_{\text{Fe}}} \rangle$ and $\langle E_{\text{tot}, V_{\text{Ni}}} \rangle$, respectively. The EIM results are calculated in the 16 384-site random structures in the magnetic ground state, and $\langle E_{\text{tot}, V_{\text{Fe}}} \rangle$ and $\langle E_{\text{tot}, V_{\text{Ni}}} \rangle$ are averaged over all the Fe and Ni sites, respectively. The DFT results suggest that $\langle E_{\text{tot}, V_{\text{Ni}}} \rangle$ decreases with increasing Ni concentration, which is also well reproduced by the EIM.

B. Temperature dependence of vacancy formation properties

The temperature evolution of G_f^{mag} in the Fe-Ni alloys with 50% and 75% Ni, where the system successively undergoes the chemical and magnetic transitions with increasing temperature, is investigated and the results are shown in Fig. 7. In the equilibrium phases, G_f^{mag} first increase with increasing temperature, then decrease abruptly across the chemical transition temperatures, and, finally, increase slowly.

This variation of G_f^{mag} is clearly related to the changes of magnetic and chemical orders in the equilibrium phases. To separate these contributions, we calculate G_f^{mag} in the structures where the chemical configurations are frozen, while the magnetic configurations are equilibrated at each temperature. It can be seen that G_f^{mag} in the equilibrium phases with 50% and 75% Ni closely follow those in the corresponding ordered structures up to 500 K and 600 K, respectively. This can be correlated with the previous results in Fig. 2, which show that these alloys remain fairly ordered up to 500 K and 600 K,

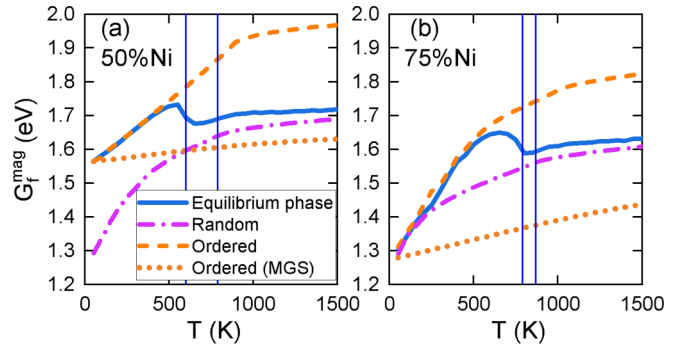


FIG. 7. G_f^{mag} as a function of temperature in the alloys with (a) 50 and (b) 75% Ni. The solid lines are obtained in the equilibrium structures and the vertical lines denote the corresponding chemical and magnetic transition temperatures. The dash-dotted (or dashed) lines are obtained in the random (or ordered) structures where the chemical order is frozen and only the magnetic order evolves with temperature. The dotted lines are obtained in the ordered structures in the magnetic ground state (both chemical and magnetic configurations are frozen).

with an ALRO > 0.96 . Near the chemical transition temperatures, G_f^{mag} in the equilibrium phases deviate the trends in the ordered structures, but approach those in the disordered phases. As G_f^{mag} are higher in the ordered structures than in the respective disordered ones, the chemical transitions thus lead to a decrease in G_f^{mag} .

Figure 7 indicates that G_f^{mag} in the ordered and disordered structures increase with increasing temperature. Such variations are related not only to magnetic excitations, but also to the changes of weights in the local vacancy formation energies. Indeed, even if the structures are chemically and magnetically frozen, G_f^{mag} still tend to increase with temperature. For example, G_f^{mag} in $L1_2$ -FeNi₃ with the magnetic ground state can be calculated as

$$\begin{aligned} G_f^{\text{mag}} &= -k_B T \ln \left[0.25 \exp \left(-\frac{E_f^{\text{Fe-lat}}}{k_B T} \right) \right. \\ &\quad \left. + 0.75 \exp \left(-\frac{E_f^{\text{Ni-lat}}}{k_B T} \right) \right], \end{aligned} \quad (10)$$

where $E_f^{\text{Fe-lat}}$ and $E_f^{\text{Ni-lat}}$ are the vacancy formation energies in the Fe and Ni sublattices given in Table IV, respectively. As suggested by the expression, the lower $E_f^{\text{Fe-lat}}$ has a dominant weight in the evaluation of G_f^{mag} at low temperatures, but $E_f^{\text{Fe-lat}}$ and $E_f^{\text{Ni-lat}}$ eventually have similar weights at high temperatures. As a result, G_f^{mag} in $L1_2$ -FeNi₃ increases from $E_f^{\text{Fe-lat}}$ at low temperature, to the arithmetic average of all local vacancy formation energies at the high-temperature limit, namely,

$$G_f^{\text{mag}} = 0.25 E_f^{\text{Fe-lat}} + 0.75 E_f^{\text{Ni-lat}} \quad \text{for } T \rightarrow +\infty. \quad (11)$$

The dotted lines in Fig. 7 denote G_f^{mag} in $L1_0$ -FeNi and $L1_2$ -FeNi₃ in the respective magnetic ground states. Comparing these results to G_f^{mag} in the same ordered structures but with the equilibrium magnetic configurations, it can be concluded that the increase of G_f^{mag} in the latter cases is

TABLE V. Solute-vacancy binding free energy (in eV) in fcc Fe and Ni in the magnetic ground state (MGS) and the PM state. The binding free energies in the intermediate temperature range lie between the values of the MGS and PM states. In our convention, a positive value indicates an attraction between the vacancy and the solute.

	Ni+V in fcc Fe		Fe+V in fcc Ni	
	1NN	2NN	1NN	2NN
MGS	0.02	0.03	-0.05	-0.03
PM (1500 K)	0.01	-0.03	-0.04	-0.07

mainly due to the magnetic excitations. More specifically, it is primarily related to the transversal spin fluctuations since the longitudinal spin fluctuations in the ordered structures are found to be relatively weak below the Curie temperatures. With additional DFT calculations, we confirm the increasing behavior of G_f^{mag} predicted by the EIM, though the magnetic disordering effects are found to be somehow exaggerated by the EIM (see the Supplemental Material [81]).

Finally, Fig. 7 shows that the variation in G_f^{mag} due to magnetic excitations occurs even at very low temperatures. This is related to the use of classical statistics instead of Bose-Einstein statistics for the spin degree of freedom [13,39]. The quantum statistics was adopted in our previous study of vacancy formation in pure fcc Fe and Ni [39]. For that, it is necessary to estimate the magnon density of states, which are configuration dependent. As alloys with various chemical orders and compositions are investigated in this study, a systematic application of quantum statistics to these configurations can be very complicated and is therefore not considered here.

C. Concentration dependence of vacancy formation properties

The predicted magnetic free energies of the Ni-vacancy binding in Fe and the Fe-vacancy binding in Ni are shown in Table V. The solute-vacancy binding free energy is defined as the following free-energy difference:

$$G_b = G(S_{N-1}V) + G(S_{N-1}X) - G(S_N) - G(S_{N-2}XV), \quad (12)$$

where S , V , X denote, respectively, host atoms, the vacancy, and the solute. The solute-vacancy interactions in Fe and Ni in the magnetic ground state are quite weak, being marginally attractive and repulsive, respectively. The magnetic transition in fcc Fe and Ni changes the binding magnetic free energy only slightly, by less than 0.04 eV. According to these results, the Ni-V interaction in fcc Fe and the Fe-V interaction in Ni are not significant at any temperature.

The predicted concentration dependence of G_f^{mag} in fcc Fe-Ni alloys at several temperatures is shown in Fig. 8. According to the calculated phase diagram, the equilibrium phases above 770 K are solid solutions for all compositions. As shown in Fig. 8, the computed G_f^{mag} at 800 K and above tends to decrease with increasing Ni concentration. This trend is also observed in the curve of G_f^{mag} at 700 K, except in the com-

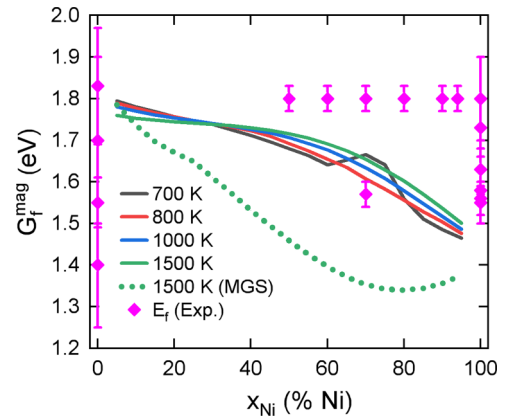


FIG. 8. The predicted G_f^{mag} as a function of Ni concentration at several temperatures, compared to the experimental vacancy formation energies (fcc Fe [102–105], fcc Ni [106–110], fcc Fe-Ni alloys [57,58]). The solid lines denote the results obtained in the equilibrium spin-atom structures, whereas the dotted line denotes the results obtained in the chemically disordered structures in the magnetic ground states (MGS), which are collinear FM above 25% Ni and noncollinear below 25% Ni (see the Supplemental Material [81]).

position range of 60–80% Ni where the alloys have an $L1_2$ ordered structure.

As shown in Fig. 8, G_f^{mag} increase weakly with increasing temperature in the disordered structures with more than 30% Ni, while the trend is reversed in the disordered structures below 30% Ni. This can be correlated with our previous results, which suggest that G_f^{mag} in fcc Fe and in Ni decreases and increases with increasing temperature, respectively [39].

The small variation of G_f^{mag} with temperature in Fig. 8 does not mean that magnetism has no impact on G_f^{mag} . Indeed, there is already a large extent of magnetic disorder at temperatures where the equilibrium chemical configurations are disordered. Therefore, the effects of thermal spin fluctuations are less significant in the disordered alloys with the equilibrium magnetic states. In Fig. 8, we also show G_f^{mag} calculated in the disordered structures in the respective magnetic ground states. They are much lower than the alloys with the equilibrium magnetic states in the concentrated composition range. As presented in Fig. 9, the difference between the two curves of G_f^{mag} at 1500 K reaches a maximum of 0.32 eV around 65% Ni, where the Curie temperature is also the highest. The latter is a sign of the magnitude of the magnetic interaction energy, which is also the strongest around 65% Ni according to our model. Indeed, it is shown that the difference between G_f^{mag} in the paramagnetic state and the ground state is closely related to the magnetic interaction energy [39].

Finally, the calculated G_f^{mag} are compared to the experimental vacancy formation energies E_f in Fig. 8. We note that the calculated G_f^{mag} and E_f are similar above 1000 K, which is in the range of temperatures where the measurements of E_f were performed. To the best of our knowledge, the measurements of E_f in fcc Fe-Ni alloys have been reported only by Caplain and Chambon using magnetic anisotropy measurements [57,58]. In their first study, measurements were performed in the disordered Fe-Ni samples with 70% Ni

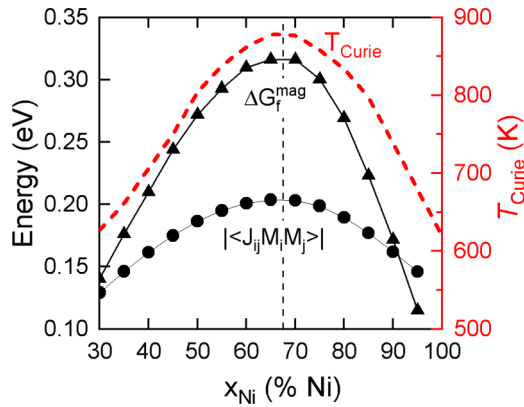


FIG. 9. Difference between G_f^{mag} in the disordered structures at 1500 K with the equilibrium magnetic states and with the magnetic ground states, the average magnetic exchange interaction energies $|\langle J_{ij} \mathbf{M}_i \mathbf{M}_j \rangle|$, and the Curie temperatures in the disordered structures.

quenched from between 873 and 973 K, and E_f was found to be 1.57 eV [57]. In their subsequent study in the disordered samples with 50% to 94% Ni quenched from above the chemical transition temperature, E_f were found to be 1.80 eV regardless of the composition [58]. It is difficult to draw a definitive conclusion regarding the concentration dependence or the values of E_f based solely on these two experiments, which could have large experimental uncertainty as in the cases of pure fcc Fe and Ni. On the other hand, our results of G_f^{mag} fall between E_f from these two sets of measurements and they are within the uncertainty of the available experimental data over the whole concentration range. It would be useful to have further experimental investigations to clarify the validity of the current predictions.

V. CONCLUSION

Phase stability and vacancy formation in fcc Fe-Ni alloys are investigated for a broad composition-temperature range, using an effective interaction model (EIM) combined with on-lattice Monte Carlo simulations.

Parametrized on DFT data only, the present EIM enables a good prediction of the experimental magnetic and chemical transition temperatures in the fcc Fe-Ni alloys over the whole range of composition. Compared with magnetic excitations, lattice vibrations show a larger impact on the chemical order-disorder transitions. The predicted fcc phase diagram is compared to the most recent CALPHAD assessment, showing an overall good agreement. In particular, the EIM predicts a phase separation in the disordered alloys around 10–40% Ni and 570–700 K, which is shown to be magnetically driven. In addition, the magnetic state has a strong influence on the chemical order-disorder transition temperature, which can differ by up to 170 K. The Curie temperature is sensitive to both atomic long-range and short-range orders, and tends to increase with increasing chemical ordering.

Vacancy formation magnetic free energy G_f^{mag} in fcc Fe-Ni alloys is studied as a function of temperature and composition. It is worth noting that the temperature evolution of G_f^{mag} in the magnetic alloys cannot be described by the Ruch model [20] or the Girifalco model [56] due to the simultaneous evolution of magnetic and chemical degrees of freedom. We find that magnetic disorder leads to an increase of G_f^{mag} , while chemical disorder has the opposite effect. In the solid solutions, G_f^{mag} tends to decrease with increasing Ni concentration. Our results reveal that the effects of magnetic excitations and transitions on vacancy formation properties are much more significant in concentrated Fe-Ni alloys than in pure Fe and Ni, due to the strong magnetic interaction in the concentrated alloys as revealed in the concentration dependence of Curie temperatures.

ACKNOWLEDGMENTS

This work was performed using DARI-GENCI resources under the Projects No. A0090906020 and No. A0110906020, and the CINECA-MARCONI supercomputer within the SISTEEL project. K.L. is supported by the CEA NUMERICS program, which has received funding from the European Union's Horizon 2020 research and innovation program under the Marie Skłodowska-Curie Grant Agreement No. 800945.

- [1] R. Soulaïrol, C. C. Fu, and C. Barreateau, *J. Phys.: Condens. Matter* **22**, 295502 (2010).
- [2] J. S. Wróbel, D. Nguyen-Manh, M. Y. Lavrentiev, M. Muzyk, and S. L. Dudarev, *Phys. Rev. B* **91**, 024108 (2015).
- [3] H. Hasegawa and D. G. Pettifor, *Phys. Rev. Lett.* **50**, 130 (1983).
- [4] M. Y. Lavrentiev, D. Nguyen-Manh, and S. L. Dudarev, *Phys. Rev. B* **81**, 184202 (2010).
- [5] P.-W. Ma, S. L. Dudarev, and J. S. Wróbel, *Phys. Rev. B* **96**, 094418 (2017).
- [6] M. Rahaman, A. V. Ruban, A. Mookerjee, and B. Johansson, *Phys. Rev. B* **83**, 054202 (2011).
- [7] A. V. Ruban, P. A. Korzhavyi, and B. Johansson, *Phys. Rev. B* **77**, 094436 (2008).
- [8] A. Schneider, C.-C. Fu, and C. Barreateau, *Phys. Rev. B* **98**, 094426 (2018).
- [9] I. Mirebeau, V. Pierron-Bohnes, C. Decorse, E. Rivière, C. C. Fu, K. Li, G. Parette, and N. Martin, *Phys. Rev. B* **100**, 224406 (2019).
- [10] Y. Iijima, K. Kimura, and K. Hirano, *Acta Metallurg.* **36**, 2811 (1988).
- [11] S. Huang, D. L. Worthington, M. Asta, V. Ozolins, G. Ghosh, and P. K. Liaw, *Acta Mater.* **58**, 1982 (2010).
- [12] H. Wen and C. H. Woo, *J. Nucl. Mater.* **470**, 102 (2016).
- [13] A. Schneider, C. C. Fu, F. Soisson, and C. Barreateau, *Phys. Rev. Lett.* **124**, 215901 (2020).
- [14] I. Abrikosov, A. Ponomareva, P. Steneteg, S. Barannikova, and B. Alling, *Curr. Opin. Solid State Mater. Sci.* **20**, 85 (2016).
- [15] S. V. Okatov, A. R. Kuznetsov, Y. N. Gornostyrev, V. N. Urtsev, and M. I. Katsnelson, *Phys. Rev. B* **79**, 094111 (2009).
- [16] L. Delczeg, B. Johansson, and L. Vitos, *Phys. Rev. B* **85**, 174101 (2012).

- [17] V. I. Razumovskiy, A. Reyes-Huamantínco, P. Puschnig, and A. V. Ruban, *Phys. Rev. B* **93**, 054111 (2016).
- [18] D. Gambino and B. Alling, *Phys. Rev. B* **98**, 064105 (2018).
- [19] A. V. Ruban and V. I. Razumovskiy, *Phys. Rev. B* **85**, 174407 (2012).
- [20] L. Ruch, D. R. Sain, H. L. Yeh, and L. Girifalco, *Solid State Commun.* **18**, vi (1976).
- [21] P.-W. Ma and S. L. Dudarev, *Phys. Rev. B* **86**, 054416 (2012).
- [22] P.-W. Ma and S. L. Dudarev, in *Handbook of Materials Modeling* (Springer International Publishing, Cham, 2020), pp. 1017–1035.
- [23] M. Y. Lavrentiev, R. Soulaïrol, C.-C. Fu, D. Nguyen-Manh, and S. L. Dudarev, *Phys. Rev. B* **84**, 144203 (2011).
- [24] M. Y. Lavrentiev, J. S. Wróbel, D. Nguyen-Manh, and S. L. Dudarev, *Phys. Chem. Chem. Phys.* **16**, 16049 (2014).
- [25] M. Y. Lavrentiev, J. S. Wróbel, D. Nguyen-Manh, S. L. Dudarev, and M. G. Ganchenkova, *J. Appl. Phys.* **120**, 043902 (2016).
- [26] L. J. Swartzendruber, V. P. Itkin, and C. B. Alcock, *J. Phase Equilib.* **12**, 288 (1991).
- [27] I. Ohnuma, S. Shimenouchi, T. Omori, K. Ishida, and R. Kainuma, *Calphad Comput. Coupl. Phase Diag. Thermochem.* **67**, 101677 (2019).
- [28] Y. Mishin, M. J. Mehl, and D. A. Papaconstantopoulos, *Acta Mater.* **53**, 4029 (2005).
- [29] G. Cacciamani, A. Dinsdale, M. Palumbo, and A. Pasturel, *Intermetallics* **18**, 1148 (2010).
- [30] G. Bonny, R. Pasianot, and L. Malerba, *Philos. Mag.* **89**, 3451 (2009).
- [31] T. Mohri, *J. Mater. Sci.* **50**, 7705 (2015).
- [32] K. Li and C.-C. Fu, *Phys. Rev. Materials* **4**, 023606 (2020).
- [33] M.-Z. Dang and D. G. Rancourt, *Phys. Rev. B: Condens. Matter Mater. Phys.* **53**, 2291 (1996).
- [34] M. Ekholm, H. Zapolsky, A. V. Ruban, I. Vernyhora, D. Ledue, and I. A. Abrikosov, *Phys. Rev. Lett.* **105**, 167208 (2010).
- [35] I. V. Vernyhora, D. Ledue, R. Patte, and H. Zapolsky, *J. Magn. Magn. Mater.* **322**, 2465 (2010).
- [36] H. Ding, V. I. Razumovskiy, and M. Asta, *Acta Mater.* **70**, 130 (2014).
- [37] N. Sandberg, Z. Chang, L. Messina, P. Olsson, and P. Korzhavyi, *Phys. Rev. B* **92**, 184102 (2015).
- [38] O. Hegde, M. Grabowski, X. Zhang, O. Waseda, T. Hickel, C. Freysoldt, and J. Neugebauer, *Phys. Rev. B* **102**, 144101 (2020).
- [39] K. Li, C.-C. Fu, and A. Schneider, *Phys. Rev. B* **104**, 104406 (2021).
- [40] H. Guan, S. Huang, J. Ding, F. Tian, Q. Xu, and J. Zhao, *Acta Mater.* **187**, 122 (2020).
- [41] X. Zhang and M. H. F. Sluiter, *Phys. Rev. B* **91**, 174107 (2015).
- [42] C. Li, J. Yin, K. Odbadrakh, B. C. Sales, S. J. Zinkle, G. M. Stocks, and B. D. Wirth, *J. Appl. Phys.* **125**, 155103 (2019).
- [43] J. B. Piochaud, T. P. C. Klaver, G. Adjanor, P. Olsson, C. Domain, and C. S. Becquart, *Phys. Rev. B* **89**, 024101 (2014).
- [44] J. Wróbel, D. Nguyen-Manh, S. Dudarev, and K. Kurzydłowski, *Nucl. Instrum. Methods Phys. Res. Sect. B Beam Interact. Mater. At.* **393**, 126 (2017).
- [45] A. Manzoor, Y. Zhang, and D. S. Aidhy, *Comput. Mater. Sci.* **198**, 110669 (2021).
- [46] S. Zhao, G. M. Stocks, and Y. Zhang, *Phys. Chem. Chem. Phys.* **18**, 24043 (2016).
- [47] J. Mayer, C. Elsässer, and M. Fähnle, *Phys. Status Solidi* **191**, 283 (1995).
- [48] M. Hagen and M. Finnis, *Philos. Mag. A* **77**, 447 (1998).
- [49] Y. Mishin and C. Herzig, *Acta Mater.* **48**, 589 (2000).
- [50] C. Woodward, M. Asta, G. Kresse, and J. Hafner, *Phys. Rev. B* **63**, 094103 (2001).
- [51] M. de Koning, C. R. Miranda, and A. Antonelli, *Phys. Rev. B* **66**, 104110 (2002).
- [52] J. Rogal, S. V. Divinski, M. W. Finnis, A. Glensk, J. Neugebauer, J. H. Perepezko, S. Schuwalow, M. H. F. Sluiter, and B. Sundman, *Phys. Status Solidi* **251**, 97 (2014).
- [53] A. V. Ruban and M. Dehghani, *Phys. Rev. B* **94**, 104111 (2016).
- [54] D. Morgan and Y. Zhang, *Phys. Rev. B* **101**, 136101 (2020).
- [55] Y. Zhang, A. Manzoor, C. Jiang, D. Aidhy, and D. Schwen, *Comput. Mater. Sci.* **190**, 110308 (2021).
- [56] L. A. Girifalco, *J. Phys. Chem. Solids* **25**, 323 (1964).
- [57] W. Chambron and A. Caplain, *Acta Metallurg.* **22**, 357 (1974).
- [58] A. Caplain and W. Chambron, *Acta Metallurg.* **25**, 1001 (1977).
- [59] A. Schneider, C.-C. Fu, O. Waseda, C. Barreteau, and T. Hickel, *Phys. Rev. B* **103**, 024421 (2021).
- [60] A. V. Ruban, S. Khmelevskiy, P. Mohn, and B. Johansson, *Phys. Rev. B* **75**, 054402 (2007).
- [61] P. E. Blöchl, *Phys. Rev. B* **50**, 17953 (1994).
- [62] G. Kresse and D. Joubert, *Phys. Rev. B* **59**, 1758 (1999).
- [63] G. Kresse and J. Hafner, *Phys. Rev. B* **47**, 558 (1993).
- [64] G. Kresse and J. Furthmüller, *Comput. Mater. Sci.* **6**, 15 (1996).
- [65] G. Kresse and J. Furthmüller, *Phys. Rev. B* **54**, 11169 (1996).
- [66] J. P. Perdew, K. Burke, and M. Ernzerhof, *Phys. Rev. Lett.* **77**, 3865 (1996).
- [67] M. Methfessel and A. T. Paxton, *Phys. Rev. B* **40**, 3616 (1989).
- [68] H. J. Monkhorst and J. D. Pack, *Phys. Rev. B* **13**, 5188 (1976).
- [69] A. Zunger, S.-H. Wei, L. G. Ferreira, and J. E. Bernard, *Phys. Rev. Lett.* **65**, 353 (1990).
- [70] J. M. Cowley, *Phys. Rev.* **77**, 669 (1950).
- [71] E. Martínez, C. C. Fu, M. Levesque, M. Nastar, and F. Soisson, *Solid State Phenom.* **172–174**, 1016 (2011).
- [72] M. Yu. Lavrentiev, C.-C. Fu, and F. Soisson, *J. Magn. Magn. Mater.* **506**, 166763 (2020).
- [73] V. T. Tran, C. C. Fu, and A. Schneider, *Comput. Mater. Sci.* **183**, 109906 (2020).
- [74] L.-Y. Tian, H. Levämäki, O. Eriksson, K. Kokko, Á. Nagy, E. K. Délczeg-Czirják, and L. Vitos, *Sci. Rep.* **9**, 8172 (2019).
- [75] J. Yin, M. Eisenbach, D. M. Nicholson, and A. Rusanu, *Phys. Rev. B* **86**, 214423 (2012).
- [76] M. Levesque, E. Martínez, C.-C. Fu, M. Nastar, and F. Soisson, *Phys. Rev. B* **84**, 184205 (2011).
- [77] O. Senninger, E. Martínez, F. Soisson, M. Nastar, and Y. Bréchet, *Acta Mater.* **73**, 97 (2014).
- [78] Y. Wang, K. Li, F. Soisson, and C. S. Becquart, *Phys. Rev. Materials* **4**, 113801 (2020).
- [79] M. Trochet, F. Soisson, C.-C. Fu, and M. Y. Lavrentiev, *Comput. Mater. Sci.* **199**, 110698 (2021).
- [80] B. Dutta, F. Körmann, S. Ghosh, B. Sanyal, J. Neugebauer, and T. Hickel, *Phys. Rev. B* **101**, 094201 (2020).

- [81] See Supplemental Material at <http://link.aps.org/supplemental/10.1103/PhysRevB.106.024106> for the model parametrization.
- [82] D. A. Kofke and E. D. Glandt, *Mol. Phys.* **64**, 1105 (1988).
- [83] L. Bergqvist and A. Bergman, *Phys. Rev. Materials* **2**, 013802 (2018).
- [84] B. Widom, *J. Chem. Phys.* **39**, 2808 (1963).
- [85] P. Sindzingre, G. Ciccotti, C. Massobrio, and D. Frenkel, *Chem. Phys. Lett.* **136**, 35 (1987).
- [86] K. Li, Magnetochemical coupling effects on thermodynamics, point-defect formation and diffusion in Fe-Ni alloys: A theoretical study, Ph.D. thesis, Université Paris-Saclay, 2021.
- [87] J. Crangle and G. C. Hallam, *Proc. R. Soc. A* **272**, 119 (1963).
- [88] H. Asano, *J. Phys. Soc. Jpn.* **27**, 542 (1969).
- [89] M. Peschard, *Rev. Métallurg.* **22**, 490 (1925).
- [90] I. A. Abrikosov, A. E. Kissavos, F. Liot, B. Alling, S. I. Simak, O. Peil, and A. V. Ruban, *Phys. Rev. B* **76**, 014434 (2007).
- [91] T. Nagata, M. Funaki, and J. Danon, *Mem. Natl. Inst. Polar Res. Spec. Issue* **41**, 364 (1986).
- [92] R. J. Wakelin and E. L. Yates, *Proc. Phys. Soc. Sect. B* **66**, 221 (1953).
- [93] T. G. Kollie and C. R. Brooks, *Phys. Status Solidi* **19**, 545 (1973).
- [94] J. Paulevé, D. Dautreppe, J. Laugier, and L. Néel, *J. Phys. le Radium* **23**, 841 (1962).
- [95] J. W. Drijver, F. Van Der Woude, and S. Radelaar, *Phys. Rev. Lett.* **34**, 1026 (1975).
- [96] J. Van deen and F. Van Der Woude, *Acta Metallurg.* **29**, 1255 (1981).
- [97] K. B. Reuter, D. B. Williams, and J. I. Goldstein, *Geochim. Cosmochim. Acta* **52**, 617 (1988).
- [98] A. Chamberod, M. Roth, and L. Billard, *J. Magn. Magn. Mater.* **7**, 101 (1978).
- [99] S. Komura, T. Takeda, and Y. Endoh, *J. Magn. Magn. Mater.* **50**, 69 (1985).
- [100] T. Takeda, S. Komura, T. Miyazaki, Y. Endoh, and S. Itoh, *J. Magn. Magn. Mater.* **70**, 431 (1987).
- [101] D. G. Rancourt, H. H. Smit, and R. C. Thiel, *J. Magn. Magn. Mater.* **66**, 121 (1987).
- [102] H.-E. Schaefer, K. Maier, M. Weller, D. Herlach, A. Seeger, and J. Diehl, *Scr. Metallurg.* **11**, 803 (1977).
- [103] C. W. Schulte, J. L. Campbell, and J. A. Jackman, *Appl. Phys.* **16**, 29 (1978).
- [104] S. M. Kim and W. J. Buyers, *J. Phys. F: Met. Phys.* **8**, L103 (1978).
- [105] H. Matter, J. Winter, and W. Triftshäuser, *Appl. Phys.* **20**, 135 (1979).
- [106] W. Wycisk and M. Feller-Kniepmeier, *J. Nucl. Mater.* **69-70**, 616 (1978).
- [107] L. C. Smedskjaer, M. J. Fluss, D. G. Legnini, M. K. Chason, and R. W. Siegel, *J. Phys. F: Met. Phys.* **11**, 2221 (1981).
- [108] J. Wolff, M. Franz, J. E. Kluin, and D. Schmid, *Acta Mater.* **45**, 4759 (1997).
- [109] H.-P. Scholz, Measurements of the absolute vacancy concentration in nickel and ordered intermetallic nickel alloys with a differential dilatometer, Ph.D. thesis, University of Göttingen, 2001.
- [110] T. Troev, C. Angelov, and I. Mincov, *Phys. Lett. A* **138**, 65 (1989).